

---

# Absolute density measurement of SD radicals in a molecular beam at the quantum-noise-limit

Arin Mizouri,<sup>a</sup> Lianzhong Deng,<sup>b</sup> Jack S. Eardley,<sup>b</sup> N. Hendrik Nahler,<sup>c</sup> Eckart Wrede,<sup>b,‡</sup> and David Carty<sup>\*a,b,‡</sup>

**The absolute density of SD radicals in a molecular beam has been measured down to  $(1.1 \pm 0.1) \times 10^5 \text{ cm}^{-3}$  in a modestly specified apparatus that uses a cross-correlated combination of cavity ring-down and laser-induced fluorescence detection. Such a density corresponds to  $215 \pm 21$  molecules in the probe volume at any given time. The quantum-noise-limited noise-equivalent absorption sensitivity of the apparatus was found to be  $(3.5 \pm 0.3) \times 10^{-11} \text{ cm}^{-1} \text{ Hz}^{-1/2}$ , based on a 200 s acquisition time at 10 Hz, therefore competing favourably with more sophisticated techniques.**

The knowledge of absolute densities of dilute molecular samples is important in a diverse range of disciplines including atmospheric chemistry and environmental pollutants monitoring,<sup>1,2</sup> combustion and automotive engineering,<sup>3,4</sup> astrochemistry,<sup>5</sup> plasma physics,<sup>6</sup> chemical reaction dynamics,<sup>7</sup> cold and ultracold molecules,<sup>8</sup> manufacturing,<sup>9</sup> radiocarbon dating,<sup>10</sup> detection of chemical weapons agents and toxic industrial chemicals and explosives<sup>11</sup> and medical diagnostics and monitoring.<sup>12</sup> Absorption techniques, such as cavity ring-down spectroscopy (CRDS), are well-established and widely used for direct quantitative measurements of molecules in gas, liquid and solid-phase samples. In particular absolute absorption coefficients  $\alpha = \sigma\rho$  are measured and, therefore, absolute densities  $\rho$  can be determined, if the absorption cross-section  $\sigma$  is known. In recent refinements of CRDS and its variants, Courtois *et al.* achieved a noise-equivalent absorption sensitivity (NEA) of  $9 \times 10^{-11} \text{ cm}^{-1} \text{ Hz}^{-1/2}$  in 500 s acquisition time using differential-CRDS<sup>13</sup> and Foltynowicz *et al.* achieved a NEA of  $1.8 \times 10^{-11} \text{ cm}^{-1} \text{ Hz}^{-1/2}$  in 400 s using NICE-OHMS.<sup>14</sup> In both of these studies IR frequency-locked narrowband CW lasers were used to measure the absorbance by species such as  $\text{CO}_2$  and  $\text{C}_2\text{H}_2$  that filled the entire cavity.

In terms of sensitivity, CRDS cannot compete with laser-induced fluorescence (LIF), which, with careful attenuation

of stray light from the incident laser and photon-counting over very long acquisition times, enables the detection of single figure numbers of molecules in the probe volume. Kirste recently measured densities as low as  $200 \text{ molecules cm}^{-3}$  (with an error around 30%) in their *ca.*  $0.03 \text{ cm}^3$  probe volume.<sup>7</sup> Unlike CRDS, LIF is not self-calibrating, so Kirste obtained absolute densities by painstakingly calibrating their detection system and fluorescence process (fluorescence quantum yield, solid angle observed by the detector, detector quantum efficiency and transmission efficiency of optical components in front of the detector).

Recently, Sanders *et al.*<sup>15</sup> described a method called cavity-enhanced laser-induced fluorescence (CELIF) that combines the absolute absorption capabilities of CRDS and the sensitivity of LIF to measure absorption coefficients of 1,4-bis(phenylethynyl)benzene over an extended dynamic range.<sup>15</sup> However, the lowest densities that could in principle have been detected were not reached due to instabilities in the source and the densities were too high to necessitate photon-counting techniques.

Here we demonstrate for the *d*-mercapto radical SD in a pulsed molecular beam, using a standard UV pulsed dye laser and a modest CRD and LIF setup, that CELIF has a limit of detection (LOD) of  $10^5 \text{ cm}^{-3}$ , which, in a  $0.002 \text{ cm}^3$  probe volume, corresponds to *ca.* 200 molecules, *i.e.* a quantum-noise-limited NEA of  $3.5 \times 10^{-11} \text{ cm}^{-1} \text{ Hz}^{-1/2}$  based on a 200 s acquisition time at 10 Hz.

Fig. 1 shows a schematic representation of our experiment. A nanosecond pulsed Nd:YAG (Continuum Surelite II-10, 532 nm, 10 Hz repetition rate) pumped dye laser (Sirah Cobra Stretch), tuned to the  $P_1(1.5)$  line of the  $(0,0)$ -band of the  $A^2\Sigma^+ \leftarrow X^2\Pi_{3/2}$  transition at 323.17 nm, is coupled via beam-shaping, mode-matching and polarisation-rotating optics into a standard ring-down cavity of length  $d = 98.29 \pm 0.05 \text{ cm}$ . The cavity mirrors (Layertec, peak reflectivity at 330 nm) have a radius of curvature of 1 m that makes a  $1/e^2$  beam waist radius of 0.023 cm. The ring-down transient is measured with a PMT (Hamamatsu, H7732-10) and digitised with an oscilloscope (LeCroy, WaveRunner 610Zi). The cavity axis, the  $x$ -axis, intersects orthogonally, 12 cm downstream, a free-jet expansion of varying densities of SD radicals seeded in 2 bar of Ne propagating along the  $z$ -axis from a pulsed solenoid

---

<sup>a</sup> Department of Physics, Durham University, South Road, Durham, DH1 3LE, United Kingdom. E-mail: david.carty@durham.ac.uk

<sup>b</sup> Department of Chemistry, Durham University, South Road, Durham DH1 3LE, United Kingdom.

<sup>c</sup> School of Engineering and Physical Sciences, Heriot-Watt University, Edinburgh EH14 4AS, United Kingdom.

‡ These authors contributed equally to this work.

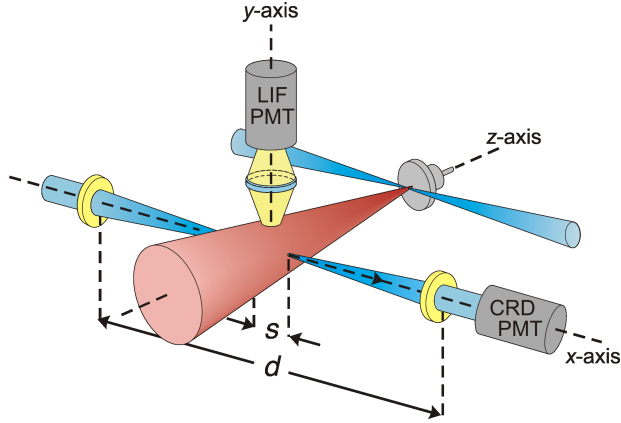


**Fig. 1** CELIF experimental setup. SD radicals generated by photodissociation of  $D_2S$  in the expansion of the supersonic beam ( $z$ -axis) are excited by the CRD laser ( $x$ -axis) and the fluorescence is detected ( $y$ -axis) simultaneously with the ring-down signal  $I^{CRD}$ .

valve (Parker, General Valve Series 9). The SD radicals are created by photodissociation of  $D_2S$ , mixed at varying partial pressures in the Ne before expansion, using an ArF excimer laser (GAM LASER, EX5, 193 nm, *ca.* 4 mJ per pulse). A three-lens LIF detection optical system is aligned along the  $y$ -axis and has a field of view that restricts the probe volume to  $1.9 \times 10^{-3} \text{ cm}^3$  over a length of  $s = 1.2 \text{ cm}$ . The LIF signal is recorded with a PMT (Hamamatsu, H3695-10) on another channel of the oscilloscope.

The methodology for CELIF has been described in detail previously.<sup>15</sup> Briefly, the time-integrated, or photon-counted, LIF signal

$$S_{SD}^{LIF} = I_{SD}^{LIF} \alpha_{SD} \Gamma_{SD} g, \quad (1)$$

where  $I_{SD}^{LIF}$  is the light intensity that has interacted with the SD radicals within the probe volume,  $\alpha_{SD} = \sigma_{SD} \rho_{SD}$  is the absorption coefficient,  $\Gamma_{SD}$  is the fluorescence quantum yield and  $\sigma_{SD}$  is the bandwidth corrected absorption cross section of the SD radicals.  $g$  is an instrument factor discussed below. For highly reflective mirrors ( $\approx 100\%$ ) and low photon loss per cavity pass (*i.e.*  $\alpha_{SD}s \ll 1$ ),  $I_{SD}^{LIF} \approx 2I^{CRD}/T$ ,<sup>15</sup> where  $I^{CRD}$  is the time-integrated CRD intensity and  $T$  is the transmission of the cavity exit mirror. Therefore, the CELIF signal

$$S_{SD}^{CELIF} = \frac{S_{SD}^{LIF}}{I_{SD}^{CRD}} = \sigma_{SD} \rho_{SD} \Gamma_{SD} \frac{2g}{T} \quad (2)$$

is the integrated LIF signal normalised shot-to-shot to the integrated CRD intensity. The factor  $g/T$  is difficult to determine because it contains factors that depend on the instrument, *i.e.*  $g$  is the product of the fraction of fluorescence photons created in the probe volume that hit the LIF PMT, the quantum efficiency of that PMT and a factor quantifying the convolution of the detection system solid angle with the angular distribution

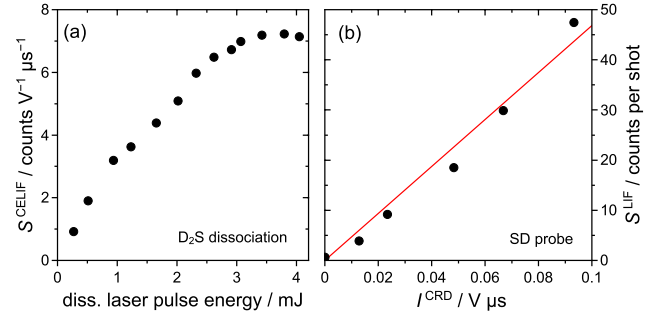


**Fig. 2** (a) Dependence of the SD CELIF signal on the pulse energy of the  $D_2S$  dissociation laser showing saturation at 3.5 mJ and above. (b) Dependence of the average LIF counts per shot on the probe laser pulse energy as measured by the time-integrated ring-down signal. The statistical error bars are smaller than the symbols.

of the fluorescence or scattering process. This latter factor is unity for an isotropic fluorescence angular distribution, or a measurement carried out on an anisotropic angular distribution at the magic angle between the laser polarisation and LIF detection axis. *Crucially* to the CELIF method, the instrument dependent factor can be calibrated using Rayleigh scattering (here done with dry  $N_2$ ), a process where  $g/T$  is the same for a magic angle measurement and the equivalent factors in eqn (2) are known, *i.e.*

$$\frac{S_{SD}^{CELIF}}{S_{N_2}^{CELIF}} = \frac{\sigma_{SD} \rho_{SD} \Gamma_{SD}}{\sigma_{N_2} \rho_{N_2} \Gamma_{N_2}}. \quad (3)$$

For Rayleigh scattering  $\Gamma_{N_2} = 1$ . On the other hand,  $\Gamma_{SD} \neq 1$ , because predissociation of the SD radical competes with fluorescence.<sup>16</sup> Therefore, equation 3 can be rearranged to give

$$\alpha_{SD} = \sigma_{SD} \rho_{SD} = \frac{\rho_{N_2}}{S_{N_2}^{CELIF}} \frac{\sigma_{N_2}}{\Gamma_{SD}} S_{SD}^{CELIF}. \quad (4)$$

The measurements of  $S_{SD}^{CELIF}$  had to take place in a regime where the photodissociation of the  $D_2S$  molecules was saturated, which ensures that any shot-to-shot instabilities or long-term drifts in the laser pulse energy do not contribute to the noise in  $S_{SD}^{CELIF}$ . Fig. 2a shows  $S_{SD}^{CELIF}$  as a function of photodissociation laser pulse energy. The signal varies linearly at low laser pulse energies and begins to enter a saturated regime at around 3.5 mJ per pulse. Unlike the photodissociation process, it is crucial that the fluorescence of SD radicals is *not* saturated for the shot-to-shot normalisation of the CELIF to be valid. Fig. 2b shows that the dependence of  $S_{SD}^{CELIF}$  on the intensity of the probe light in the cavity is linear thus proving that the experiment is not in the LIF saturation regime. The probe laser intensity was reduced sufficiently to ensure that the number of signal counts was not under-represented due to photon coincidences on the detector.

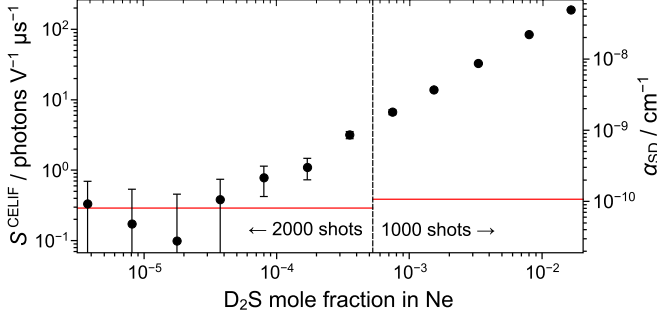


**Fig. 3** Determination of the limit of detection of the SD CELIF measurement and, therefore, of  $\alpha_{SD}$  by successive dilution of the  $D_2S/Ne$  gas mixture.

Fig. 3 shows a plot of  $S_{SD}^{CELIF}$  versus the mole fraction of  $D_2S$  mixed in the Ne carrier gas before expansion. Starting from the highest value, the mole fraction is lowered by sequentially diluting the previous mixture by pumping away a fraction of the 2 bar total pressure and adding Ne until the total pressure returned to 2 bar. After each dilution, the gas mixture was “stirred” for 20 minutes using convection currents generated by heating two loops of pipe of unequal length each entering the bottom and exiting the top of the gas mixing bottle feeding the solenoid valve.

The data manipulation procedure that was used in the analysis was as follows. The number of photon counts on the LIF PMT  $S_{tot,i}^{LIF}$  for each  $i$ th shot was recorded for  $n$  laser shots to give the “total” signal counts originating from SD molecules and from background sources. The total CELIF signal  $S_{tot,i}^{CELIF} = S_{tot,i}^{LIF}/I_{tot,i}^{CRD}$  was calculated for each  $i$ th shot using  $I_{tot,i}^{CRD} = A_{0,i}^{CRD}\tau_i$ , where  $A_{0,i}^{CRD}$  and  $\tau_i$  are the amplitude and ring-down time of the  $i$ th CRD transient, respectively, both obtained from an exponential fit. The average total CELIF signal per shot  $S_{tot}^{CELIF}$ , the average ring-down intensity per shot  $I_{tot}^{CRD}$  and the average counts on the LIF PMT  $S_{tot}^{LIF}$ , were then used in subsequent calculations. The error  $\delta I_{tot}^{CRD}/I_{tot}^{CRD}$  is *ca.* 1% and is dominated by the error in  $\tau_i$  and the error  $\delta S_{tot}^{LIF} = (S_{tot}^{LIF}/n)^{1/2}$  comes from Poisson statistics. The error in  $S_{tot}^{CELIF}$  is therefore

$$\delta S_{tot}^{CELIF} = \left[ \frac{1}{nS_{tot}^{LIF}} + \left( \frac{\delta I_{tot}^{CRD}}{I_{tot}^{CRD}} \right)^2 \right]^{1/2} S_{tot}^{CELIF}. \quad (5)$$

After recording the total counts over  $n$  laser shots for each dilution, the photodissociation laser was blocked and the average background signal per shot  $S_{bg}^{LIF}$  measured over another  $n$  laser shots.  $S_{bg}^{CELIF}$  and  $\delta S_{bg}^{CELIF}$  were then determined using the same procedure as above.  $\delta S_{bg}^{CELIF}$  is given by an expression equivalent to eqn (5), except that, because  $S_{bg}^{LIF}$  is very small, the error is dominated by the quantum-noise term,

which is the first term in the square-root. The average CELIF signal per shot originating from SD molecules is determined by the background subtraction  $S_{SD}^{CELIF} = S_{tot}^{CELIF} - S_{bg}^{CELIF}$ .

To derive an expression for the limit of detection (LOD) of the CELIF signal, the approximation that  $I_{tot}^{CRD} = I_{bg}^{CRD} = I^{CRD}$  is made such that the error in the SD LIF counts is

$$\delta S_{SD}^{LIF} = (S_{SD}^{LIF} + 2S_{bg}^{LIF})^{1/2} n^{-1/2}. \quad (6)$$

The LOD is reached when the LIF signal-to-noise ratio is unity,<sup>17</sup> *i.e.*  $S_{SD}^{LIF} = S_{SD}^{LIF,LOD} = \delta S_{SD}^{LIF}$ , which, when substituted into eqn (6) and solving for  $S_{SD}^{LIF,LOD}$ , gives, in the limit of large  $n$ ,

$$S_{SD}^{LIF,LOD} \simeq \left( \frac{2S_{bg}^{LIF}}{n} \right)^{1/2}. \quad (7)$$

The CELIF signal at the LOD is therefore

$$S_{SD}^{CELIF,LOD} \simeq \left( \frac{2S_{bg}^{LIF}}{n(I^{CRD})^2} \right)^{1/2}. \quad (8)$$

Comparing eqn (8) to the background equivalent of eqn (5) reveals that

$$S_{SD}^{CELIF,LOD} \simeq \sqrt{2} \delta S_{bg}^{CELIF}, \quad (9)$$

if the error in  $I^{CRD}$  is considered negligible. The horizontal line in Fig. 3 is calculated using eqn (9) with  $n = 1000$  shots and  $n = 2000$  shots at the higher and lower  $D_2S$  mole fractions, respectively.

On Fig. 3, the  $S_{SD}^{CELIF}$  axis has been converted into  $\alpha_{SD}$  using eqn (4). The ratio  $\rho_{N_2}/S_{N_2}^{CELIF}$  was measured to be  $(1.31 \pm 0.02) \times 10^{15}$  counts per shot  $V \mu s cm^{-3}$  from the inverse of the slope of the number density dependence of the  $N_2$  Rayleigh scattering, which is shown in Fig. 4. The slope and the error were determined from a linear  $\chi^2$  fit. The same procedure as described above to evaluate  $S_{SD}^{CELIF}$ , and associated errors, was also used to evaluate the average  $N_2$  Rayleigh scattering CELIF signal per shot  $S_{N_2}^{CELIF}$  and its error  $\delta S_{N_2}^{CELIF}$ , with the exception that no background subtraction was required as it did not affect the slope of the graph in Fig. 4.

As per the SD CELIF measurements, the probe laser intensity was reduced sufficiently to ensure good photon counting statistics. The  $N_2$  pressures in the chamber above and below 48 mbar were measured using a calibrated piezo transducer gauge (Pfeiffer Vacuum, APR 265) and a calibrated Pirani gauge (Pfeiffer Vacuum, PBR 260), respectively. Pressures were converted into densities via the van der Waals equation. In principle, the  $N_2$  pressure could have been measured using the CRDS signal, however, the cavity was found not to be stable as the  $N_2$  pressure was changed. The total error  $\delta S_{N_2}^{CELIF}$  is dominated by the quantum-noise  $\delta S_{N_2}^{LIF}$  at low pressures and by  $\delta I_{N_2}^{CRD}$  at high pressures.

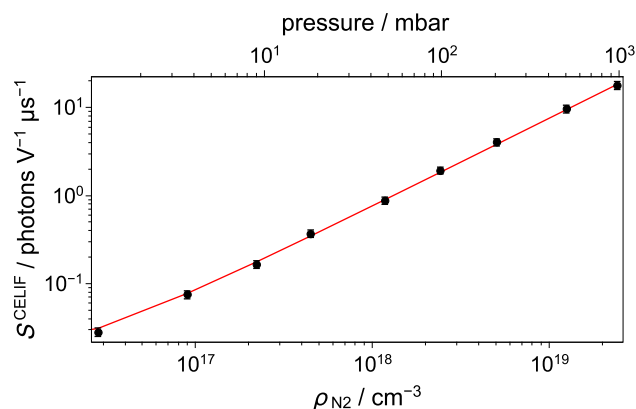


**Fig. 4** Determination of the ratio  $\rho_{N_2}/S_{N_2}^{CELIF}$  from measurements of the CELIF signal from  $N_2$  Rayleigh scattering at varying  $N_2$  pressures.

The minimum detected absorption coefficient according to eqn (4) is,  $\alpha_{SD}^{LOD} = (7.9 \pm 0.6) \times 10^{-11} \text{ cm}^{-1}$ , using the values  $\sigma_{N_2}(323.17 \text{ nm}) = (4.1 \pm 0.2) \times 10^{-26} \text{ cm}^2$ ,<sup>18</sup> and  $\Gamma_{SD} = 0.20 \pm 0.01$ .<sup>16,19</sup> PGOPHER<sup>20</sup> was used, inputting known spectroscopic constants,<sup>21–23</sup> to obtain a cross section for SD of  $(4.5 \pm 0.2) \times 10^{-15} \text{ cm}^2 \text{ GHz}$ . Using a measured laser bandwidth of  $(6.4 \pm 0.3) \text{ GHz}$ , the bandwidth corrected cross section is  $\sigma_{SD} = (7.0 \pm 0.5) \times 10^{-16} \text{ cm}^2$ . The noise at the LOD is dominated by the quantum-noise in the LIF signal, therefore, the quantum-noise-limited NEA<sup>24</sup> for this experiment is given by

$$\text{NEA} = \alpha_{SD}^{LOD} \left( \frac{2}{f_{\text{rep}}} \right)^{1/2} = (3.5 \pm 0.3) \times 10^{-11} \text{ cm}^{-1} \text{ Hz}^{-1/2}. \quad (10)$$

The density of SD radicals at our LOD is  $\rho_{SD}^{LOD} = 1.1 \times 10^5 \text{ molecules cm}^{-3}$  and has an error of only 10%. Given the very small probe volume, this density corresponds to an average of just  $215 \pm 21$  molecules in the probe volume at any given time.

The NEA in these CELIF experiments compares favourably with the D-CRDS<sup>13</sup> and NICE-OHMS<sup>14</sup> techniques. It should be noted that the CELIF technique is limited to molecules that fluoresce on a timescale less than the time it takes for a molecule to traverse the probe volume and that the molecule absorbs in a wavelength region  $> 220 \text{ nm}$  where CRD mirrors can be fabricated. However, many important molecules of interest in many fields fall into this category (e.g. NO).

Given the modest setup used in these experiments, there is much room to improve the NEA. Examining the background equivalent of eqn (5) reveals that maximising  $n$  and/or minimising  $S_{bg}^{LIF}$  and  $\delta I_{bg}^{CRD}/I_{bg}^{CRD}$  will lower the LOD of the experiment. Even though the cavity is an effective discriminator of scattered light compared to a standard LIF setup, 99%

of  $S_{bg}^{LIF}$  originates from scattered light from the probe laser, most likely from UV fluorescence of the cavity entrance mirror UV grade fused silica substrate. Thin mirrors with a low absorbance allied with light baffles and low reflectivity surfaces inside the cavity chamber, as is done routinely in standard LIF measurements, could effectively eliminate the scattered light leaving only dark counts on the PMT as the source of background signal. A photon-counting PMT (e.g. Hamamatsu H7360-01, 2 pA dark current) could lower the dark counts by a further factor of  $10^3$ . The result would thus be to lower the NEA to a value on the order of  $10^{-13} \text{ cm}^{-1} \text{ Hz}^{-1/2}$  and the LOD density to ca.  $4 \times 10^2 \text{ cm}^{-3}$  (on average less than 1 molecule in the probe volume at any given time). Using a narrow bandwidth laser of, say, 120 MHz<sup>7</sup> would not change the NEA, but would increase the bandwidth corrected SD absorption cross-section by a factor of 50 and commensurately lower the LOD density to  $< 10 \text{ cm}^{-3}$ . The narrower bandwidth laser would also excite only a single mode of the cavity, which, in conjunction with the use of a 14-bit digitiser card, would allow a better determination of the ring-down time and amplitude thus lowering  $\delta I_{bg}^{CRD}/I_{bg}^{CRD}$  with the effect of lowering the LOD yet further.<sup>24</sup>

This work was supported by the EPSRC [grant no. EP/I012044/1]. NHN thanks the Royal Society for a University Research Fellowship. The authors would like to thank G. Meijer, S. Y. T. van de Meerakker, T. Momose and S. Willitsch for useful discussions.

## References

- 1 D. Stone, L. K. Whalley and D. E. Heard, *Chem. Soc. Rev.*, 2012, **41**, 6348–6404.
- 2 A. Fried, G. Diskin, P. Weibring, D. Richter, J. G. Walega, G. Sachse, T. Slate, M. Rana and J. Podolske, *Appl. Phys. B-Lasers Opt.*, 2008, **92**, 409–417.
- 3 I. Rahinov, A. Goldman and S. Cheskis, *Combustion and Flame*, 2006, **145**, 105–116.
- 4 R. M. Spearrin, C. S. Goldenstein, J. B. Jeffries and R. K. Hanson, *Meas. Sci. Technol.*, 2013, **24**, 055107.
- 5 M. A. Blitz and P. W. Seakins, *Chem. Soc. Rev.*, 2012, **41**, 6318–6347.
- 6 A. A. Ionin, I. V. Kochetov, A. P. Napartovich and N. N. Yuryshev, *J. Phys. D, Appl. Phys.*, 2007, **40**, R25–R61.
- 7 M. Kirste, *PhD thesis*, Fritz-Haber-Institut der Max-Planck-Gesellschaft and Freien Universitaet, Berlin, Germany, 2012.
- 8 D. Wang, B. Neyenhuis, M. H. G. de Miranda, K.-K. Ni, S. Ospelkaus, D. S. Jin and Y. J., *Phys. Rev. A*, 2010, **81**, 061404.
- 9 J. Booth, G. Cunge, L. Biennier, D. Romanini and Kachanov, *Chem. Phys. Lett.*, 2000, **317**, 631–636.
- 10 I. Galli, S. Bartalini, S. Borri, P. Cancio, D. Mazzotti, P. De Natale and G. Giusfredi, *Phys. Rev. Lett.*, 2011, **107**, 270802.
- 11 C. K. N. Patel, *Eur. Phys. J. Special Topics*, 2008, **153**, 1–18.
- 12 F. M. Schmidt, O. Vaitinen, M. Metsala, M. Lehto, C. Forsblom, P.-H. Groop and L. Halonen, *J. Breath Res.*, 2013, **7**, 017109.
- 13 J. Courtois, K. Bielska and J. T. Hodges, *J. Opt. Soc. Am. B*, 2013, **30**, 1486–1495.

- 
- 14 A. Foltynowicz, I. Silander and O. Axner, *J. Opt. Soc. Am. B*, 2011, **28**, 2797–2805.
  - 15 S. E. Sanders, O. R. Willis, N. H. Nahler and E. Wrede, *J. Chem. Phys.*, *Submitted*, 2013.
  - 16 M. D. Wheeler, A. J. Orr-Ewing and M. N. R. Ashfold, *J. Chem. Phys.*, 1997, **107**, 7591–7600.
  - 17 G. Hancock and V. L. Kasyutich, *Appl. Phys. B*, 2004, **79**, 383–388.
  - 18 D. Itayakov, H. Linnartz and W. Ubachs, *Mol. Phys.*, 2008, **106**, 2471–2479.
  - 19 M. Kawasaki, H. Sato, G. Inoue and M. Suzuki, *J. Chem. Phys.*, 1989, **91**, 6758–6764.
  - 20 C. M. Western, PGOPHER, *a Program for Simulating Rotational Structure*, University of Bristol, <http://pgopher.chm.bris.ac.uk>.
  - 21 D. A. Ramsay, *J. Chem. Phys.*, 1952, **20**, 1920–1927.
  - 22 J. Senekowitsch, H. J. Werner, P. Rosmus, E. A. Reinsch and S. V. O’Neil, *J. Chem. Phys.*, 1985, **83**, 4661–4667.
  - 23 E. Klisch, T. Klaus, S. Belov, A. Dolgner, R. Schieder, G. Winnewisser and E. Herbst, *Astrophys. J.*, 1996, **473**, 1118–1124.
  - 24 R. D. van Zee, J. T. Hodges and J. P. Looney, *Appl. Opt.*, 1999, **38**, 3951–3960.
-